Article

Evidence of abnormal hot carrier thermalization at van Hove singularity of twisted bilayer graphene

Nianze Shang [a,b,1], Chen Huang [a,1], Qing Chen [c,1], Chang Liu [a], Guangjie Yao [a], Zhipei Sun [b], Sheng Meng [c,*], Kaihui Liu [a,d,*], Hao Hong [a,e,*]

[a] State Key Laboratory for Mesoscopic Physics, Frontiers Science Center for Nano-optoelectronics, School of Physics, Peking University, Beijing 100871, China
[b] QTF Centre of Excellence, Department of Electronics and Nanoengineering, Aalto University, Espoo 02150, Finland
[c] Institute of Physics, Chinese Academy of Sciences, Beijing 100190, China
[d] Songshan Lake Materials Lab, Institute of Physics, Chinese Academy of Sciences, Dongguan 523808, China
[e] Interdisciplinary Institute of Light-Element Quantum Materials and Research Centre for Light-Element Advanced Materials, Peking University, Beijing 100871, China

ARTICLE INFO

ABSTRACT

Interlayer twist evokes revolutionary changes to the optical and electronic properties of twisted bilayer graphene (TBG) for electronics, photonics and optoelectronics. Although the ground state responses in TBG have been vastly and clearly studied, the dynamic process of its photoexcited carrier states mainly remains elusive. Here, we unveil the photoexcited hot carrier dynamics in TBG by time-resolved ultrafast photoluminescence (PL) autocorrelation spectroscopy. We demonstrate the unconventional ultrafast PL emission between the van Hove singularities (VHSs) with a ∼4 times prolonged relaxation lifetime. This intriguing photoexcited carrier behavior is ascribed to the abnormal hot carrier thermalization brought by bottleneck effects at VHSs and interlayer charge distribution process. Our study on hot carrier dynamics in TBG offers new insights into the excited states and correlated physics of graphene twistronics systems.

1. Introduction

In the past decades, hot carriers in graphene have been exhaustively studied and exploited in various fields. Owing to the unique linear band structure, the carriers in graphene are endowed with very rapid carrier-carrier scattering assisted by strong Coulomb interaction [1–3]. After excitation, the intraband carrier scattering first impels photoexcited electrons and holes to thermalize independently among the conduction and valence bands with unequal chemical potentials ($\mu_e \neq \mu_h$), which grants graphene the capability of population inversion and stimulated emission [4,5]. Then the interband carrier scattering process gradually drives hot carriers to reach thermal equilibrium with an electronic temperature of up to ∼3000 K, and extends their distribution among the whole energy band at a timescale of ∼30 fs [5–7]. Finally, hot carriers experience further cooling and relaxation via scattering with opti-

cal phonons (∼100 fs) and acoustic phonons (∼1 ps) [8–10]. These various relaxation paths of hot carriers lead to diverse ultrafast phenomena in graphene. For example, the recombination of hot electron-hole pairs brings out broadband ultrafast photoluminescence (PL), which has been used as a broadband white light source [11,12]. The ultrafast and efficient hot carrier harvesting among graphene and various semiconducting materials has been fully studied with potential applications for high-energy conversion [13–18]. And the hot carrier scattering process can overcome the vacuum barrier due to strong electron–electron interaction and serve as a source of hot electron emission [19]. These intriguing carrier dynamic behaviors and the diverse ultrafast phenomena make graphene an excellent platform for advanced optoelectronics and photonics [20–24].

As a unique engineering method for two-dimensional (2D) materials, interlayer twisting brings new opportunities in both fundamental physics and applications into grapheme [25–28]. For relatively large angles, twisted bilayer graphene (TBG) manifests novel properties, including the enhanced density of states, intensified light absorption and strongly bound excitons, all emerging at the van Hove singularities (VHSs) induced by inter-

---

* Corresponding authors.
  E-mail addresses: smeng@iphy.ac.cn (S. Meng), khliu@pku.edu.cn (K. Liu), haohong@pku.edu.cn (H. Hong).
  [1] These authors contributed equally to this work.

layer interaction and band reconstruction [29–31]. As the twist angle is progressively reduced, the strong correlation of electrons leads to further marvelous discoveries in magic-angle TBG, such as the flat bands in the mini-Brillouin zone, correlated insulating states, superconductivity, ferromagnetism, and topological phase transition [32–37]. With all these fascinating optical and electronic properties, TBG-like 2D material systems have infused new vitality to the research frontiers of materials science and condensed matter physics. However, research until now on TBG is limited to the ground state, and the photoexcited state dynamical properties of TBG, representing one of the irreplaceable aspects of its physical picture and cornerstone for its application design, are still little studied.

The main challenge to probe the hot carrier dynamics in TBG can be attributed to the complexity of the transient absorption spectroscopy towards TBG circumstance (in particular, at the VHS), although it has been widely used in monolayer graphene (MLG) [2,4]. In MLG, the carrier relaxation lifetime can be inferred by transient absorption dynamics by resolving the intraband-interband absorption competing mechanism. However, the energy band reconstruction introduces intersubband transition, and the emergence of VHS in the density of states complicate the weight of intra- and inter-band contribution, which all hinder the deciphering of the exact carrier relaxation lifetime in TBG [10,38]. Moreover, the carrier dynamics of the VHS in TBG is entangled with free carriers of the same energy level on the linear bands, and it is challenging to isolate the VHS contribution in the transient absorption dynamics.

Here, we propose the time-resolved PL autocorrelation method to unveil the ultrafast hot carrier dynamics in TBG. As ultrafast PL intensity is linearly correlated with the transient hot carrier density, time-resolved PL autocorrelation should be a faithful reflection to the carrier dynamics [12,39]. Meanwhile, by extracting the peak components from PL spectra, which represent the pure VHS contribution, we can successfully recover the VHS carrier dynamics from the carrier mixture. We find that the ultrafast hot carriers on the linear bands of TBG behave similarly to MLG, while the carriers captured by VHS possess decelerated dynamics, which is 4-time longer than that of MLG. Further time-dependent density functional theory (TDDFT) suggests that the prolonged lifetime is attributed to the abnormal hot carrier thermalization brought by bottleneck effect at mini-gaps and interlayer charge redistribution process in real space. Moreover, such thermalization process is asymmetric between electrons and holes, which have different relaxation lifetimes.

2. Materials and methods

2.1. Sample fabrication

The MLG is obtained by mechanical exfoliation from HOPG bulk crystals onto a 90 nm SiO_2/Si substrate. Then we carry out the dry-transfer process on our home-built 2D material transfer stage. Using a PPC membrane/PDMS structure as a stamp, we first pick up ~20 nm thick h-BN flake, and then pick up half of the MLG sample with the h-BN flake. After fine rotation of the remaining graphene sample by rotational stage, we finally release the h-BN/graphene from the stamp onto the remaining graphene. The whole h-BN/TBG sample is then annealed in Ar/H_2 atmosphere at 400 °C for 8 h to remove the residual PPC.

2.2. Spectroscopy measurement

For PL spectra measurement, Ti:sapphire oscillator (Coherent Vitara laser) with femtosecond pulses (~25 fs, 80 MHz, 820 nm) is used to excite the ultrafast PL of TBG. The pump laser is focused onto the sample by a Cassegrain objective to avoid possible chirp-induced pulse stretching. The PL signal is collected by the same objective and detected by a spectrometer (Princeton Acton SP2500). A 750 nm short-pass filter is used to eliminate the pump signal. For the differential reflectance spectra, a supercontinuum laser source (YSL, 400–2600 nm, 1 MHz, 10 ps) is used as the excitation, and the reflection signal is also collected by a spectrometer (Princeton Acton SP2500). The reflection signal of the substrate is also collected to calculate the differential reflectance.

2.3. Time-resolved ultrafast PL spectroscopy

Ti:sapphire oscillator (Coherent Vitara laser) is used to conduct the ultrafast PL autocorrelation measurement. The output beam is split by an optical 50:50 beamsplitter, and the light path of one beam is controlled by a motorized delay stage to introduce a time delay. Then two beams are focused onto the sample by a Cassegrain objective. A BBO crystal is used to yield traditional interferometric autocorrelation second-harmonic signal, so that we can monitor the final pulse width when they reach the samples. Prism pairs are used as chirp compensation to compress the pulse width until the final width is controlled as shorter than 30 fs. After that, we monitor the PL signals of TBG and record a series of spectra under different time delays. The autocorrelation traces are obtained by integrating the spectral fluences of the certain wavelength range from the spectra of different time delays.

2.4. Calculation

The ground-state properties of TBG are calculated based on DFT using VASP software [40,41]. We use a Moiré-supercell with an optimized lattice constant of 10.79 Å. The supercell contains two graphene layers twisted at an angle of 13.2°, with an interlayer distance of 3.4 Å. A vacuum space of 20 Å is introduced along the z-axis, perpendicular to the surface. The Brillouin zone is sampled by $5 \times 5 \times 1$ k-point mesh for calculations. We utilize plane-wave basis sets with a cut-off energy of 500 eV and employ the norm-conserving pseudopotential to describe the interaction between valence electrons and ions and use the Perdew–Burke–Ernzerhof (PBE) functional with the generalized gradient approximation (GGA) to calculate the exchange–correlation energy [42]. The total energy converges to within 10^{-8} eV for all calculations.

We perform time-dependent density functional theory molecular dynamics (TDDFT-MD) simulations using the time-dependent *ab-initio* packages (TDAP) as implemented in the SIESTA software [43–45]. Due to the use of different software, the interlayer distance slightly decreased to 3.23 Å after relaxation, which satisfies the force convergence criterion of 0.005 eV/Å. The van der Waals interactions between layers are considered using the DFT-D3 method. The basis set consists of numerical atomic orbitals with double zeta polarization (DZP), and the electron-nuclear interaction is described by Troullier-Martins pseudopotentials. We utilize an auxiliary real-space grid equivalent to a plane-wave cutoff of 300 Ry and apply a $4 \times 4 \times 4$ k-mesh to sample the Brillouin zone. In order to simulate the thermalization process of carriers, we analyze the electronic structure of TBG by artificially inverting the population: we remove electrons from the valence band and self-consistently fill them into the conduction band at the M point. Subsequently, the time-dependent Kohn-Sham wavefunctions of TBG evolve in the NVE ensemble at 300 k for up to 800,000 attoseconds (800 fs) with a time step of 50 attoseconds. Throughout the real-time evolutions, the nonadiabatic couplings (i.e., the correlated electron–phonon dynamics beyond the Born-Oppenheimer approximation) are governed by the Ehrenfest theorem.

3. Results and discussion

3.1. Ultrafast PL spectroscopy

In our experiments, TBG samples with different twist angles are prepared by dry-transfer method onto a 90 nm SiO_2/Si substrate (Fig. 1a, b). Under pulsed laser excitation, photoexcited hot carriers in graphene will be scattered to high energy and generate a broadband ultrafast PL (Fig. 1c). The representative ultrafast PL spectra of MLG and TBG (with a twist angle of ~11°) under the same experimental conditions are shown in Fig. 1d. Compared to the monotonous curve of MLG, TBG shows a clear peak. For a more intuitive view, we extract the peak signal from the broad ultrafast PL background by subtracting a baseline spectrum inspired by that of the MLG (Fig. 1e). This PL peak's position evolves correspondingly with the twist angles (Fig. 1f), indicating that it is highly correlated with VHS. These results agree well with previous reports which used photoluminescence excitation spectra [46], meanwhile they are different to photoluminescence excitation spectra because the latter only reflects the absorptivity and contains no signature of the excited carriers. We note that, such peak only exists for up-conversion with low photon energy pump and vanishes as excited by high photon energy pulses (with energy larger than the peak, Fig. S1 online). Fig. 1e shows the comparison of differential reflectance spectrum and ultrafast PL spectrum for a 11° TBG sample. The extracted PL peak position is located at ~2.03 eV, in sharp contrast to a much higher reflectance peak at ~2.10 eV. Such obvious deviation can be observed for TBG samples with different twist angles (Fig. S2 online). Generally, in the thermal radiation model assuming a unified electron temperature, the emission of ultrafast PL can be described according to the generalized Kirchhoff's Law [47], where the emissivity will be proportional to absorptivity. However, it is difficult to reproduce a well-fitted PL spectrum by the absorption spectra, even considering the Fano resonance and the substrate-induced multireflection effects, due to the large deviation between reflectance and PL peaks [48].

To determine the origin of the ultrafast PL peaks in TBG, we carry out the excitation power and photon energy-dependent PL measurements. Fig. 2a shows the 2D plot of the extracted PL peak spectra under different excitation powers. The peak position remains unchanged over a wide excitation power range (Fig. S3 online). The integrated total PL fluence and extracted peak fluence exhibit $\sim I^{1.8}$ power-dependence, similar to that of MLG (Fig. 2b). The observed nonlinear dependency in the up-conversion PL can be principally ascribed to the carrier-carrier scattering processes after excitation. It necessitates the absorption of photons in excess of a singular equivalent number to facilitate the generation of electron-hole pairs at the elevated energy state. As the density of photoexcited carriers follows a linear dependence on the excitation power within the first ~30 fs [1], we believe that the nonlinear PL process involving carrier multiplication and Auger process occurs after the complex carrier scattering processes, which can strongly alter the luminescence behavior of the thermally equilibrated carriers to the nonlinearity regime [3,9]. The excitation photon energy-dependent PL spectra are carried out by tuning the excitation photon energy from 1.14 to 1.68 eV, with the excitation fluence kept the same at 0.59 mJ cm^{-2} (Fig. 2c). The spectra remain the same line shape, and the peak fluences show no obvious differences (Fig. 2d). This indicates that the population of hot carriers scattered to the PL peak emission states is almost independent of the excitation photon energy. Similar results also appear in cryogenic experiments at 7 K (Fig. S4 online). Therefore, we can safely conclude that the hot carrier recombination around VHS of TBG mostly occurs at least 30 fs after excitation, when the free carriers have reached thermal equilibrium among the entire Dirac cone.

3.2. Time-resolved PL autocorrelation

The post-thermal-equilibrium feature allows us to analyze the detailed hot carrier dynamics of TBG at VHSs by time-resolved ultrafast PL autocorrelation spectroscopy with a resolution of ~25 fs. As illustrated in Fig. 3a, two laser beams with a time delay are focused on the samples and the ultrafast PL signals are recorded by a spectrometer equipped with a charge-coupled device (See Supplementary materials for details). The time-resolved PL spectra of TBG and MLG show highly time-delay dependent feature, where the PL intensity decreases correspondingly with time-delay t (Fig. 3b). For an obvious view, with different integration choices, we can obtain autocorrelation traces regarding to carriers of different energies and momentums. We integrate the PL intensity of TBG and MLG under two different spectral ranges (I_1 (490–550 nm) refers to the range away from VHSs, and I_2 (580–630 nm) for the range resonant to VHSs, as shown in Fig. 3b) and draw their traces versus time-delay (Fig. 3c, d). As the integrated PL intensity of graphene is approximately proportional to the peak value of $n(E)$, which denotes the density of electrons (holes) at state E above (below) the Dirac point, the time-resolved PL fluence can be treated as a linear mapping to the dynamical carrier density $n(t, E)$ at time t after the pulsed laser excitation. Therefore, the carrier lifetime can be directly deciphered by exponential fitting to the PL fluence autocorrelation traces. For the range I_1, TBG and MLG both show an identical lifetime of ~150 fs (Fig. 3c). For the range I_2, we find a longer lifetime for TBG as $\tau^1_{TBG} = $ ~190 fs, and $\tau^1_{MLG} = $ ~150 fs for MLG (Fig. 3d). In TBG, this lifetime is contributed by two parts, free carriers on the linear band and carriers linked to VHSs. To separate these two parts and determine the pure carrier lifetime at VHSs, we extract the PL peak intensity at the VHS (as method in Fig. 1e) and plot its autocorrelation trace. The pure carrier lifetime at VHSs is determined to be $\tau_{VHS} = $ ~600 fs (Fig. 3e), much longer than the carrier-optical phonon scattering at the linear bands of both TBG and MLG. Moreover, τ_{VHS} is almost independent of the excitation power, in contrast to that of τ_{MLG} which decreases with the incident power in our experiments (Fig. S5 online). This anomalous behavior also indicates the abnormal carrier dynamic process at the VHSs.

3.3. TDDFT calculation

In the following, we conduct the TDDFT simulations to comprehend the complex carrier evolution in TBG. TBG with a 13.2° inter-layer twist angle is chosen as it is the commensurate Moiré superlattice close to our experimental samples. First, we calculate the exact band structure of TBG superlattices in the folded Brillouin Zone, which is conducted in a single super-cell containing 76 carbon atoms (Fig. S6a online). Providing the symmetric valence and conduction bands around the Dirac point, the symmetry-allowed transition X_{13} and X_{24} will degenerate ($X_{13} = E_3 - E_1$, $X_{24} = E_4 - E_2$, Fig. 1c) [49]. However, the conduction and valence band of graphene is in fact not symmetric, especially when the momentum approaches the M point of Brillouin Zone, due to the differences in electron-electron many-body interaction in the occupied and empty states. Such asymmetry leads to non-degenerate transition energy of X_{13} and X_{24} in TBG in our calculation, where X_{13} holds a lower transition energy and stronger oscillation strength.

Then, we simulate the dynamics at the VHS states using TDDFT method. As illustrated in Fig. 4a, the hot carriers excited by the photon energy below the VHS transition experience an ultrafast thermalization process among the linear-dispersion bands. For
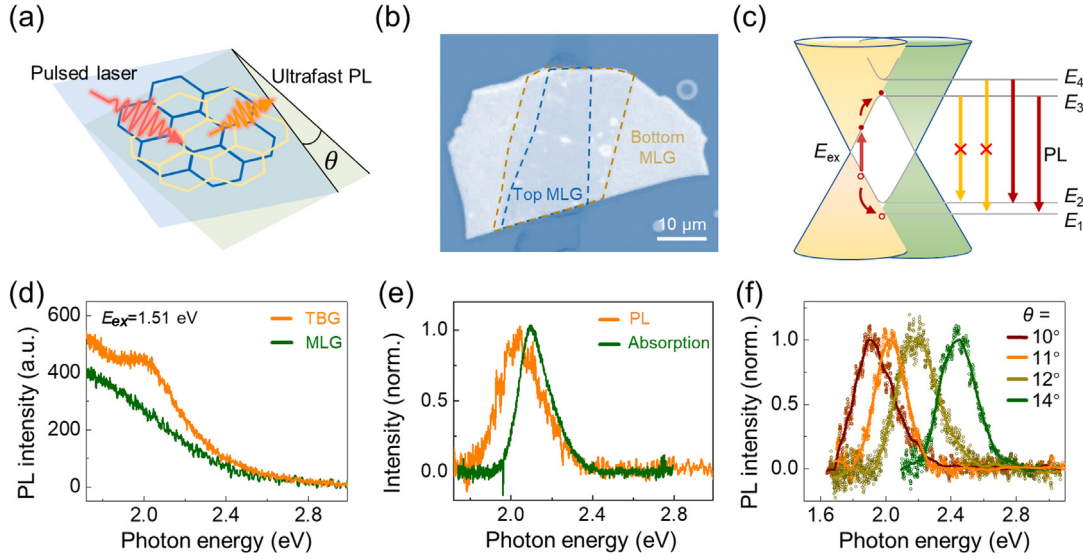
Fig. 1. (Color online) The VHS dominating ultrafast PL of TBG. (a) Schematic representation of TBG under pulse laser excitation. (b) Optical image of the 11° TBG heterostructure, with BN encapsulated on the top. (c) Schematic of TBG's up-converted PL generated at VHS formed by two intersecting Dirac cones in reciprocal space. Only the non-degenerate transitions $X_{13} = E_3 - E_1$, $X_{24} = E_4 - E_2$ are allowed according to optical selection rules. (d) Ultrafast PL spectra of TBG and MLG excited with a 1.51 eV pulsed laser. An obvious peak appears in the spectrum of TBG. (e) The extracted ultrafast PL peak of 11° TBG and the corresponding differential reflectance spectrum. The PL peak position exhibits a red-shift of ∼70 meV compared with the absorption peak. (f) The ultrafast PL peaks of TBG with several representative twist angles (10°, 11°, 12°, 14°). The PL peak position shows a clear dependence on the twist angles.
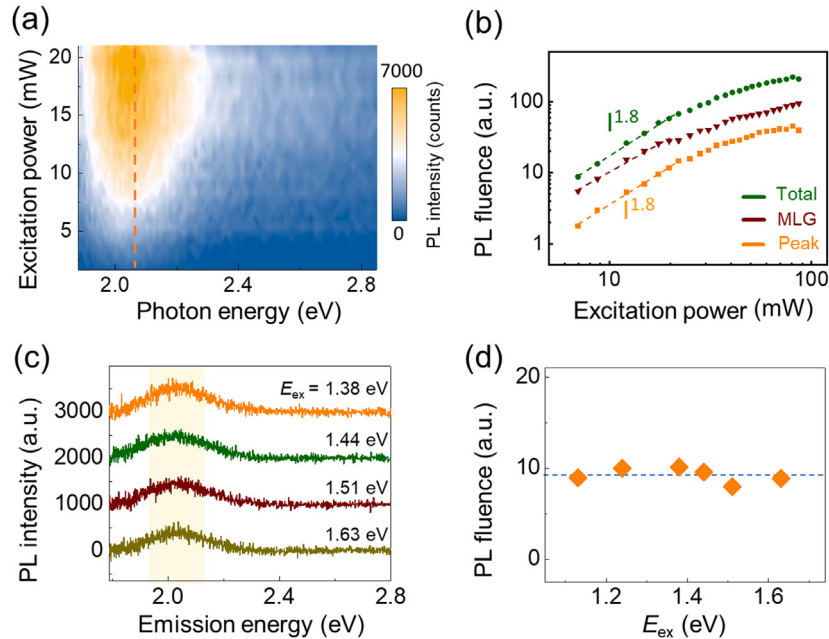

Fig. 2. (Color online) The excitation power and photon energy dependent ultrafast PL spectra. (a) The excitation power-dependent extracted PL spectra of TBG. The dash line represents the center of the ultrafast PL peaks. (b) Excitation power dependent ultrafast PL intensity in MBG and TBG. The total ultrafast PL fluence of MLG (wine) and TBG (olive, integrated before peak extraction), and the extracted peaks' fluence (orange, extracted peaks) at VHS increase nonlinearly with the excitation power. A similar nonlinear dependence is observed. (c) The ultrafast PL peak intensity of TBG under different excitation photon energies E_{ex}. (d) The integrated PL peak fluence, as denoted with the orange area in (c), versus E_{ex}. No obvious variation can be observed.

MLG, such a process dominated by intraband or interband elastic carrier scattering will drive carriers to reach an equilibrium among the whole bands at the timescale $\tau_{e-e} <$ 30 fs [9]. For TBG, however, due to the large momentum and energy disparity at VHS, hot carriers in the isolated bands (marked in green in Fig. 4a, b) can hardly be excited by either interband or intraband scattering. It means that the thermalization of TBG is sufficiently blocked by the opening bandgap at VHS. The scattering process between E_3 (E_2) and E_4

(E_1) facilitated by phonons becomes the dominating channel for the hot electron (hole) generation in the isolated bands beyond VHS. According to our calculation, the hot holes scattering process from E_2 to E_1 remains ultrafast in a timescale of ∼50 fs (Fig. S7 online), while the hot electrons scattering process from E_3 to E_4 is extended to a timescale of $\tau_{3-4} = 650$ fs (Fig. 4c, d). The asymmetric dynamical process of electrons and holes may stem from the non-identical coupling strength with phonons [50].
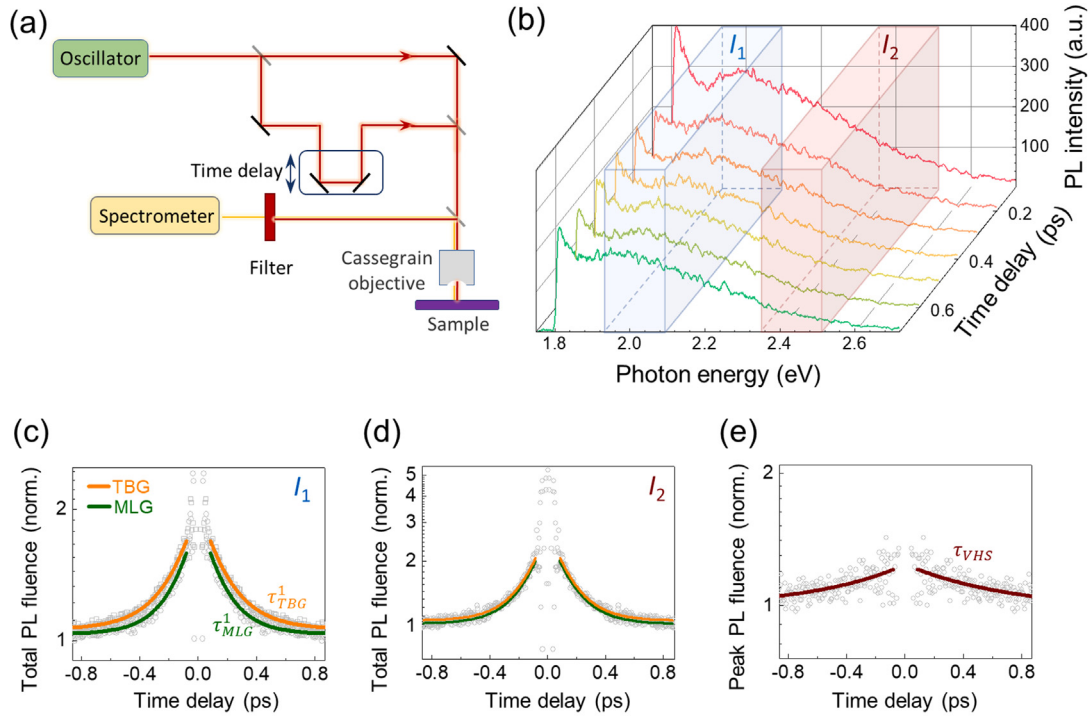
Fig. 3. (Color online) The time-resolved PL autocorrelation results. (a) Illustration of the ultrafast PL autocorrelation system. (b) The collected ultrafast PL autocorrelation spectra of TBG under a series of delay times. I_1 and I_2 indicate different integral ranges whose energy is away from VHS (I_1) or resonant to VHS (I_2). (c, d) The ultrafast PL autocorrelation traces of TBG and MLG away from VHS (c), and resonant to VHS (d). Under resonance at VHS, the relaxation lifetime of TBG and MLG is quite different with $\tau_{TBG}^1 = \sim 190$ fs and $\tau_{MLG}^1 = \sim 150$ fs. (e) The extracted pure carrier lifetime of TBG at VHS. It gives a lifetime $\tau_{VHS} = \sim 600$ fs, ~ 4 times longer than free hot carriers in MLG.
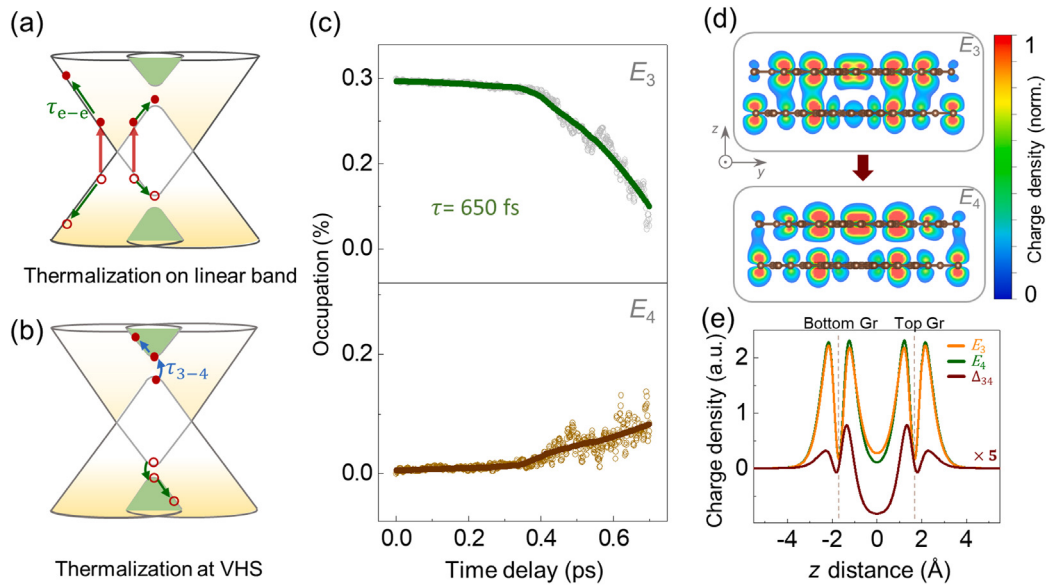

Fig. 4. (Color online) The abnormal long-term thermalization at VHS. (a) Schematics of the photoexcitation and hot carrier thermalization on the linear bands. (b) Schematics of the thermalization between VHS E_3 and E_4 facilitated by phonon scattering. (c) TDDFT calculated electron occupation evolution of E_3 (top panel) and E_4 (bottom panel). The lifetime when occupation drops to $1/e$ is about 650 fs, indicating an abnormal long-term thermalization lifetime. (d) The calculated charge density distribution in real space for a TBG supercell. The top panel illustrates the real-space distribution of E_3, and the bottom panel illustrates E_4. The interlayer charge density distribution exhibits a noticeable difference. (e) The averaged charge density along the z-axis (out of plan) in TBG. The differential charge density distribution Δ_{34} (the difference between E_4 and E_3) reveals a clear interlayer charge redistribution process.

The electron blocking at E_3, together with the lower transition energy and stronger oscillation strength of X_{13}, make it directly dominate the PL emission with prolonged lifetime at VHS. Furthermore, as the carrier lifetime of VHS is different from that of the linear bands, there will be no signature of Fano resonance in the PL spectra as we experimentally measured. Considering the absorption spectra are contributed by both X_{13} and X_{24}, with substantial Fano resonance to the continuum spectra, meanwhile the PL spectra are solely contributed by X_{13}, we believe this is the reason for the red-shifted PL peaks compared to the absorption. Moreover,

this also responds for the increased energy splitting between peaks of PL and absorption with twist angle increases, as shown in Fig. S2 (online). We note that, the phonon bottleneck effect also exists under higher pump photon energy excitation, where the electrons will accumulate at E_4. Meanwhile, the oscillation strength of X_{24} is markedly weak, resulting an undetectable signal in our experiments.

To further elucidate the origin of the prolonged thermalization τ_{3-4}, we calculate the real-space localized charge density of E_3 and E_4, as illustrated in Fig. 4d. Compared to E_4, the carrier density of E_3 is more delocalized with many carriers distributed between two graphene layers. For a clearer perspective, we calculate the average charge density along the z-axis in the real space for E_4 and E_3, and plot their difference denoted as Δ_{34} (Fig. 4e). The difference curve Δ_{34} directly reflects the gain (positive) and loss (negative) of charge during thermalization in real space. A noticeable charge density redistribution can be spotted, where carriers diffuse from inter-layer space onto the graphene layers. We conclude that this charge redistribution process and the bottleneck effect emerging at the VHS mini gaps should be the main reasons for the abnormal long-term thermalization process observed in our ultrafast PL autocorrelation spectroscopy.

4. Conclusion

In summary, we have investigated the ultrafast excited state dynamics in TBG under the influence of interlayer couplings. Using time-resolved ultrafast PL autocorrelation spectroscopy, we have detected an abnormal long-term thermalization process triggered by interlayer interaction at the VHS mini-bands. Our exploration should have important implications for the design of TBG-based ultrafast photonics and optoelectronics devices, such as light-harvesting, light-sensing or light-emitting devices. Meanwhile, our technique should be a unique spectroscopy method to investigate the fundamental element interaction in TBG at small twist angles, when the system lies in a strong-correlation regime at a cryogenic environment. We expect that the abnormal dynamics at VHS will bring more intriguing physics to TBG and its family.

Conflict of interest

The authors declare that they have no conflict of interest.

Author contributions

Hao Hong, Kaihui Liu, and Sheng Meng conceived and supervised the projects. Nianze Shang performed the device fabrication. Nianze Shang and Chen Huang performed the ultrafast spectroscopy and time-resolved PL autocorrelation experiments. Qing Chen contributed the theoretical calculations. Guangjie Yao, Chang Liu, and Zhipei Sun suggested the optical experiments. All the authors discussed and contributed to writing the paper.

References

[1] Breusing M, Kuehn S, Winzer T, et al. Ultrafast nonequilibrium carrier dynamics in a single graphene layer. Phys Rev B 2011;83:153410.
[2] Brida D, Tomadin A, Manzoni C, et al. Ultrafast collinear scattering and carrier multiplication in graphene. Nat Commun 2013;4:1987.
[3] Tomadin A, Brida D, Cerullo G, et al. Nonequilibrium dynamics of photoexcited electrons in graphene: Collinear scattering, auger processes, and the impact of screening. Phys Rev B 2013;88:035430.
[4] Li T, Luo L, Hupalo M, et al. Femtosecond population inversion and stimulated emission of dense Dirac fermions in graphene. Phys Rev Lett 2012;108:167401.
[5] Gierz I, Petersen JC, Mitrano M, et al. Snapshots of non-equilibrium Dirac carrier distributions in graphene. Nat Mater 2013;12:1119–24.
[6] Tse W-K, Das SS. Energy relaxation of hot Dirac fermions in graphene. Phys Rev B 2009;79:235406.
[7] Gierz I, Calegari F, Aeschlimann S, et al. Tracking primary thermalization events in graphene with photoemission at extreme time scales. Phys Rev Lett 2015;115:086803.
[8] Kampfrath T, Perfetti L, Schapper F, et al. Strongly coupled optical phonons in the ultrafast dynamics of the electronic energy and current relaxation in graphite. Phys Rev Lett 2005;95:187403.
[9] Butscher S, Milde F, Hirschulz M, et al. Hot electron relaxation and phonon dynamics in graphene. Appl Phys Lett 2007;91:203103.
[10] Malard LM, Fai Mak K, Castro Neto AH, et al. Observation of intra- and inter-band transitions in the transient optical response of graphene. New J Phys 2013;15:015009.
[11] Lui CH, Mak KF, Shan J, et al. Ultrafast photoluminescence from graphene. Phys Rev Lett 2010;105:127404.
[12] Liu W-T, Wu SW, Schuck PJ, et al. Nonlinear broadband photoluminescence of graphene induced by femtosecond laser irradiation. Phys Rev B 2010;82:081408.
[13] Tisdale WA, Williams KJ, Timp BA, et al. Hot-electron transfer from semiconductor nanocrystals. Science 2010;328:1543–7.
[14] Hong H, Zhang J, Zhang J, et al. Ultrafast broadband charge collection from clean graphene/$CH_3NH_3PbI_3$ interface. J Am Chem Soc 2018;140:14952–7.
[15] Chen YZ, Li YJ, Zhao YD, et al. Highly efficient hot electron harvesting from graphene before electron-hole thermalization. Sci Adv 2019;5:eaax9958.
[16] Aeschlimann S, Rossi A, Chavez-Cervantes M, et al. Direct evidence for efficient ultrafast charge separation in epitaxial WS_2/graphene heterostructures. Sci Adv 2020;6:eaay0761.
[17] Fu S, du Fosse I, Jia X, et al. Long-lived charge separation following pump-wavelength-dependent ultrafast charge transfer in graphene/WS_2 heterostructures. Sci Adv 2021;7:eabd9061.
[18] Ma H, Shang N, Liang J, et al. Enhanced hot carrier up-conversion in graphene by quantum dot coating. Adv Opt Mater 2021;10:2101563.
[19] Rezaeifar F, Ahsan R, Lin Q, et al. Hot-electron emission processes in waveguide-integrated graphene. Nat Photon 2019;13:843–8.
[20] Sun D, Aivazian G, Jones AM, et al. Ultrafast hot-carrier-dominated photocurrent in graphene. Nat Nanotechnol 2012;7:114–8.
[21] Liu CH, Chang YC, Norris TB, Zhong Z. Graphene photodetectors with ultra-broadband and high responsivity at room temperature. Nat Nanotechnol 2014;9:273–8.
[22] Tielrooij KJ, Piatkowski L, Massicotte M, et al. Generation of photovoltage in graphene on a femtosecond timescale through efficient carrier heating. Nat Nanotechnol 2015;10:437–43.
[23] Zhang Y, Huang D, Shan YW, et al. Doping-induced second-harmonic generation in centrosymmetric graphene from quadrupole response. Phys Rev Lett 2019;122:047401.
[24] Kim L, Kim S, Jha PK, et al. Mid-infrared radiative emission from bright hot plasmons in graphene. Nat Mater 2021;20:805–11.
[25] Li G, Luican A, Lopes dos Santos JMB, et al. Observation of van Hove singularities in twisted graphene layers. Nat Phys 2009;6:109–13.
[26] Bistritzer R, MacDonald AH. Moire bands in twisted double-layer graphene. Proc Natl Acad Sci USA 2011;108:12233–7.
[27] Sboychakov AO, Rakhmanov AL, Rozhkov AV, et al. Electronic spectrum of twisted bilayer graphene. Phys Rev B 2015;92:075402.
[28] Zhang WJ, Wang QX, Chen Y, et al. Van der Waals stacked 2D layered materials for optoelectronics. 2D Mater 2016;3:022001.
[29] Havener RW, Liang Y, Brown L, et al. van Hove singularities and excitonic effects in the optical conductivity of twisted bilayer graphene. Nano Lett 2014;14:3353–7.
[30] Patel H, Havener RW, Brown L, et al. Tunable optical excitations in twisted bilayer graphene form strongly bound excitons. Nano Lett 2015;15:5932–7.
[31] Patel H, Huang L, Kim CJ, et al. Stacking angle-tunable photoluminescence from interlayer exciton states in twisted bilayer graphene. Nat Commun 2019;10:1445.
[32] Cao Y, Fatemi V, Demir A, et al. Correlated insulator behaviour at half-filling in magic-angle graphene superlattices. Nature 2018;556:80–4.

[33] Cao Y, Fatemi V, Fang S, et al. Unconventional superconductivity in magic-angle graphene superlattices. Nature 2018;556:43–50.

[34] Sharpe AL, Fox EJ, Barnard AW, et al. Emergent ferromagnetism near three-quarters filling in twisted bilayer graphene. Science 2019;365:605–8.

[35] Jiang Y, Lai X, Watanabe K, et al. Charge order and broken rotational symmetry in magic-angle twisted bilayer graphene. Nature 2019;573:91–5.

[36] Xie Y, Pierce AT, Park JM, et al. Fractional Chern insulators in magic-angle twisted bilayer graphene. Nature 2021;600:439–43.

[37] Choi Y, Kim H, Peng Y, et al. Correlation-driven topological phases in magic-angle twisted bilayer graphene. Nature 2021;589:536–41.

[38] Pogna EAA, Miao XC, von Dreifus D, et al. Angle-tunable intersubband photoabsorption and enhanced photobleaching in twisted bilayer graphene. Nano Res 2021;14:2797–804.

[39] O'Haver TC, Winefordner JD. Derivation of expression for integrated luminescence intensity when using pulsing techniques in luminescence spectrometry. Anal Chem 1966;38:1258–60.

[40] Kresse G, Furthmuller J. Efficient iterative schemes for *ab initio* total-energy calculations using a plane-wave basis set. Phys Rev B 1996;54:11169–86.

[41] Kresse G, Furthmuller J. Efficiency of *ab-initio* total energy calculations for metals and semiconductors using a plane-wave basis set. Comp Mater Sci 1996;6:15–50.

[42] Perdew JP, Burke K, Ernzerhof M. Generalized gradient approximation made simple. Phys Rev Lett 1996;77:3865–8.

[43] Lion C, Guan MX, Hu SQ, et al. Photoexcitation in solids: first-principles quantum simulations by real-time TDDFT. Adv Theor Simul 2018;1:1800055.

[44] Xian L, Kennes DM, Tancogne-Dejean N, et al. Multiflat bands and strong correlations in twisted bilayer Boron Nitride: Doping-induced correlated insulator and superconductor. Nano Lett 2019;19:4934–40.

[45] You PW, Chen DQ, Lian C, et al. First-principles dynamics of photoexcited molecules and materials towards a quantum description. Wires Comput Mol Sci 2021;11:e1492.

[46] Alencar TV, von Dreifus D, Moreira MGC, et al. Twisted bilayer graphene photoluminescence emission peaks at van Hove singularities. J Phys-Condens Mat 2018;30.

[47] Wurfel P. The chemical-potential of radiation. J Phys C Solid State 1982;15:3967–85.

[48] Ghirardini L, Pogna EAA, Soavi G, et al. Tunable broadband light emission from graphene. 2D Mater 2021;8:035026.

[49] Moon P, Koshino M. Optical absorption in twisted bilayer graphene. Phys Rev B 2013;87:205404.

[50] Choi YW, Choi HJ. Strong electron-phonon coupling, electron-hole asymmetry, and nonadiabaticity in magic-angle twisted bilayer graphene. Phys Rev B 2018;98:241412.

Qing Chen received his bachelor's degree in Applied Physics from Hunan University, currently pursuing a Ph.D. degree in Condensed Matter Physics at the Institute of Physics, Chinese Academy of Sciences. His main research area is exciton dynamics and time-dependent density functional theory software development.
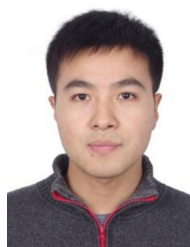
Sheng Meng is a researcher at the Institute of Physics, Chinese Academy of Sciences, and director of the State Key Laboratory of Surface Physics. His research area is surface quantum interactions, excited state quantum dynamics, microscopic mechanisms of energy conversion and storage, solar cells, atomic-scale properties of water, etc.

Kaihui Liu is now a professor at School of Physics, Peking University. As the fellow of National Science Fund for Distinguished Young Scholars, he and his group are pioneering in the studies of growth mechanism and spectral physics for low-dimensional materials.

Nianze Shang received his bachelor's degree from Beihang University in 2018, and Ph.D. degree at School of Physics, Peking University in 2023. He now works as a postdoctroal researcher at Aalto University, Finland. His research interest is nonlinear optics and ultrafast spectroscopy for 2D materials.

Hao Hong received his bachelor's degree from Shandong University in 2013, and Ph.D. degree at Peking University in 2020. Now he works as an assistant professor at School of Physics, Peking University. His research interest is time-resolved ultrafast spectroscopy and nonlinear spectroscopy of low-dimensional nanomaterials.

Chen Huang received his bachelor's degree in Physics in 2020 from Peking University, currently pursuing a Ph.D. degree in Condensed Matter Physics at School of Physics, Peking University. His main research interest is ultrafast and nonlinear spectroscopy of 2D materials.